Rapid Communications

# Optical perturbation of the hole pockets in the underdoped high-$T_c$ superconducting cuprates

S. Freutel,[1] J. D. Rameau,[2,*] L. Rettig,[1,†] I. Avigo,[1] M. Ligges,[1] Y. Yoshida,[3] H. Eisaki,[3] J. Schneeloch,[2] R. D. Zhong,[2] Z. J. Xu,[2] G. D. Gu,[2] U. Bovensiepen,[1,‡] and P. D. Johnson[2,§]

[1]*Fakultät für Physik, Universität Duisburg-Essen, 47048 Duisburg, Germany*

[2]*Condensed Matter Physics and Materials Science Division, Brookhaven National Laboratory, Upton, New York 11973, USA*

[3]*National Institute of Advanced Industrial Science & Technology, Tsukuba, Ibaraki 305-8568, Japan*

(Received 4 September 2018; revised manuscript received 1 February 2019; published 22 February 2019)

The high-$T_c$ superconducting cuprates are recognized as doped Mott insulators. Several studies indicate that as a function of doping and temperature, there is a crossover from this regime into a phase characterized as a marginal Fermi liquid. Several calculations of the doped Mott insulating phase indicate that the Fermi surface defines small pockets which at the higher doping levels switch to a full closed Fermi surface, characteristic of a more metallic system. Here we use femtosecond laser-based pump-probe techniques to investigate the structure of the Fermi surface in the underdoped region of $Bi_2Sr_2CaCu_2O_{8+\delta}$ and compare it with that associated with the optimally doped material. We confirm the concept of a small pocket in the underdoped system consistent with theoretical predictions in this strongly correlated state.

DOI: 10.1103/PhysRevB.99.081116

It is well established that the ground states of the parent cuprate materials are antiferromagnetic insulators. Upon doping, long-range magnetic order is lost and replaced by superconductivity with transition temperatures previously thought unattainable. However, the phase diagram is also dominated by the so-called pseudogap regime where, at high temperatures, the system has a gap in the spectral response centered around the chemical potential with maximum in the antinodal direction. At low temperatures, the system enters the superconducting state. It is therefore generally thought that a determination of the source of the pseudogap and the subsequent unraveling of the complexities of the cuprate phase diagram will ultimately provide a pathway to a final understanding of the physics of high-$T_c$ superconductivity and, from that, a possible pathway to the development of new materials with even higher superconducting transition temperatures. As such, the pseudogap represents one of the most studied regions of the cuprate phase diagram. Early photoemission studies found this region to be characterized by arcs centered in the nodal direction reflecting the presence of the gap in the antinodal region [1,2]. Some studies indicate a temperature dependence to the arc length [3], others an arc length influenced primarily by the doping level [4,5]. More detailed studies of the states above the chemical potential identified a particle-hole asymmetry in the pseudogap state [4] with the latter subsequently shown to be consistent with hole pockets having an area proportional to the doping level [6]. In this picture, the pockets are formed by the arcs on one side and a "ghost" Fermi surface of reduced intensity or invisible on the backside as found in theories that treat the strong correlations associated with the doping of a Mott insulator [7–9]. The possibility of an invisible backside reflects the local value of the Green's function being zero at the chemical potential, a concept associated with the Mott insulator [10]. We note that the system can also be described by models of the charge transfer insulator (CTI) type that take account of the excitation energies associated with the ligand oxygen atoms [11]. Under certain conditions, the CTI and Mott insulators can be shown to be equivalent [12]. Support for such models also comes from spectroscopic intensity scanning tunneling microscopy (SISTM) or quasiparticle interference studies of the Fermi surface reconstruction [13] and from high magnetic field studies of the charge carrier count [14]. The latter study was in fact carried out on yttrium barium copper oxide (YBCO), but both studies are again consistent with a Fermi surface reconstruction such that the "enclosed" Fermi surface area switches from scaling with the doping level $x$ in the underdoped region to $(1+x)$ in the overdoped region at a critical doping level, $x_c$, approximately equal to 0.19. A critical doping level of approximately 0.19 in bismuth strontium calcium copper oxide (BSCCO) is also consistent with several other studies including Raman [15] and thermodynamic considerations [16]. We further note the particle-hole asymmetry reported in the earlier photoemission studies [4], which has also been noted in a recent pump-probe photoemission study of the same system [17]. Questions remain, however, about the nature of the arcs. Are they really one side of a "pocket" that scales with $x$ or do they, for instance, reflect the thermal closing in the vicinity of the node of a $d$-wave gap associated with preformed pairs. In the latter case, the arc would be part of a Fermi surface that scales with an area given by $(1+x)$, reflecting the observation that the parent compound has a half-filled band leading to one hole already in the ground state. In the present study, we therefore return to these questions

*Present address: Physical Sciences Inc., Andover, Massachusetts 01810, USA.

†Present address: Fritz-Haber-Institute of the Max-Planck-Society, Faradayweg 4-6, 14195 Berlin, Germany.

‡uwe.bovensiepen@uni-due.de

§pdj@bnl.gov

 

but now use pump-probe techniques to photodope rather than chemical dope to modify the hole concentration. By pumping additional holes into the system and monitoring the change in the momentum-dependent Fermi wave vectors around the arc on femtosecond timescales, we are able confirm a picture of small "hole pockets" in the pseudogap region.

The experimental system used in this study at the University of Duisburg-Essen combines a commercial regeneratively amplified Ti:sapphire laser system (Coherent RegA 9040) and a homebuilt time-of-flight (TOF) electron spectrometer employing a position-sensitive delay line anode (Roentdek Hexanode). With this unique instrument, we measure the photoelectron intensity as a function of kinetic energy, two independent in-plane momentum directions $k_x$ and $k_y$, and pump-probe delay $t$ [18]. Time-resolved experiments were performed in a pump-probe geometry by first exciting the samples using the fundamental $p$-polarized (perpendicular to the nodal line) output of our laser system ($h\nu_{\text{pump}} = 1.5\,\text{eV}$, 40 fs pulse duration, 6 μJ energy per pulse) and subsequently probing the pump-induced dynamics by direct photoemission using suitably delayed frequency-quadrupled $s$-polarized (parallel to the nodal line) pulses ($h\nu_{\text{probe}} = 6.0\,\text{eV}$, 90 fs pulse duration). The fundamental and frequency-quadrupled pulse trains at a 250 kHz repetition rate were focused on the sample to $(100\,\mu\text{m})^2$ and $(50\,\mu\text{m})^2$, respectively. The temporal overlap between pump and probe pulses was determined with an accuracy of $\Delta t_0 = \pm 5\,\text{fs}$ by analyzing hot carrier relaxation as a function of time delay in $Bi_2Sr_2CaCu_2O_{8+\delta}$ in energy windows $E$–$E_F$ = 1.4–1.5 eV above the Fermi level $E_F$. Here we work at pump fluences of a few $100\,\mu\text{J/cm}^2$ as specified below. The subsequent population dynamics showed negligible hot carrier lifetime contributions, thus directly reflecting the pump-probe cross correlation (XC) which is found to have a width of $100 \pm 5$ fs.

Angle-resolved photoemission spectra (ARPES) were recorded as four-dimensional data sets $I\,(E, k_x, k_y, t)$ with exposure times of 60 s in 20 subsequent scans by time- and angle-resolved photoemission spectroscopy (tr-ARPES). The probe-pulse intensity was carefully tuned to prevent spectral broadening due to space-charge effects, resulting in typical electron count rates of 100 kHz at the electron analyzer. The Fermi energy $E_F$ was referenced at $T = 100 \pm 5$ K to a 2.8-nm-thick Pb film evaporated onto the samples using a calibrated Knudsen cell at the end of the measurement. Fitting of the Fermi- Dirac distribution yielded a Gaussian energy resolution of $\Delta E = 55 \pm 5\,\text{meV}$ full width at half maximum as confirmed separately by the probe beam's optical spectrum. Thus the overall temporal, spectral, and momentum resolutions of the experiment were determined to be below 100 fs, 55 meV, and $2 \times 10^{-3}$ Å$^{-1}$, respectively. Single-crystal samples of $Bi_2Sr_2CaCu_2O_{8+\delta}$ grown using standard floating-zone furnace techniques were cleaved *in situ* under ultrahigh-vacuum conditions ($p$<10–10 mbar) at base temperatures of 100 K.

Figure 1 shows the essential elements of the experiment. As previously noted, within certain theories, in the underdoped regime, the Fermi surface is thought to be composed of pockets with one side having spectral weight in the form of arcs and the other side essentially invisible to spectral

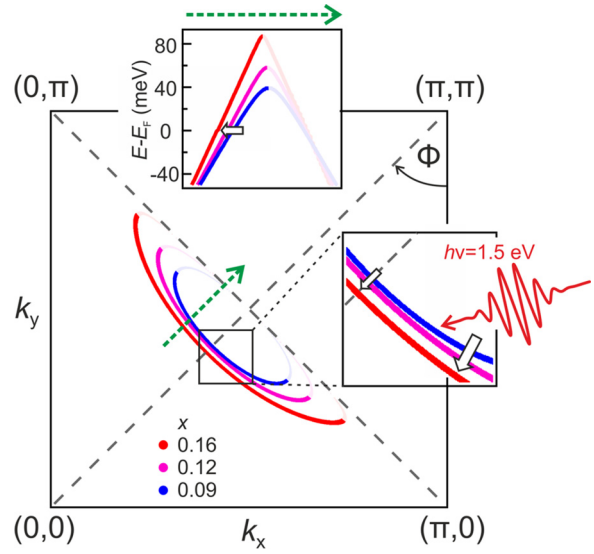


FIG. 1. The Fermi surface calculated within the framework of the YRZ ansatz as a function of the doping levels indicated. The upper inset shows how the concept of "closed" pockets arises from this type of model. The right-hand inset shows the effect on the Fermi surface of photodoping by pumping with IR (1.5 eV) in the present experiment.

probes [8]. The formation of such pockets as a function of doping is shown in the upper inset. Essentially, a particle-hole asymmetry manifests in the form of a parabolic dispersion with the two sides of the parabola defining the two sides of the pocket at the chemical potential. The top of the parabola or peak in dispersion is defined by the scattering of the photohole in the underlying spin liquid associated with resonating valence bond (RVB)-type models [8,19]. Again, as noted earlier, alternative models that recognize the strong correlations in the system can also produce the pockets [7,9], as can models based on the concept of pair density waves [20]. Pumping with the near-IR pulses temporarily introduces more holes into the system, resulting in a short-lived expansion of the Fermi surface [21] or pocket, as indicated in the inset to the right of Fig. 1.

Figure 2(a) shows the Fermi surface for optimally doped Bi2212 ($T_c = 91$K) as measured directly in the TOF spectrometer at negative time delays before pumping. The measured Fermi surface on the left represents the integration of two separate measurements approximately symmetric around the nodal point. Here the sample temperature is 100 K and the fluence $200\,\mu\text{J/cm}^2$. As reported before [20], and reflecting the sudden injection of charge, Fig. 2(b) shows the shift in momentum of the dispersing band at a binding energy 15 meV below the Fermi level as recorded 100 fs after the pump pulse, and Fig. 2(c) compares the dispersion of the entire band in the nodal direction before the pump pulse, at $t = 0$ and at $t = 100$ fs after the pump pulse when the displacement due to additional holes is at its maximum.

Figure 3 shows the detected change in the Fermi wave vector as a function of angle and time for two different samples: the optimally doped material ($T_c = 91$ K) and the underdoped sample ($T_c = 50$ K). Again, in both cases, the sample is held at a temperature of 100 K and the incident fluence is

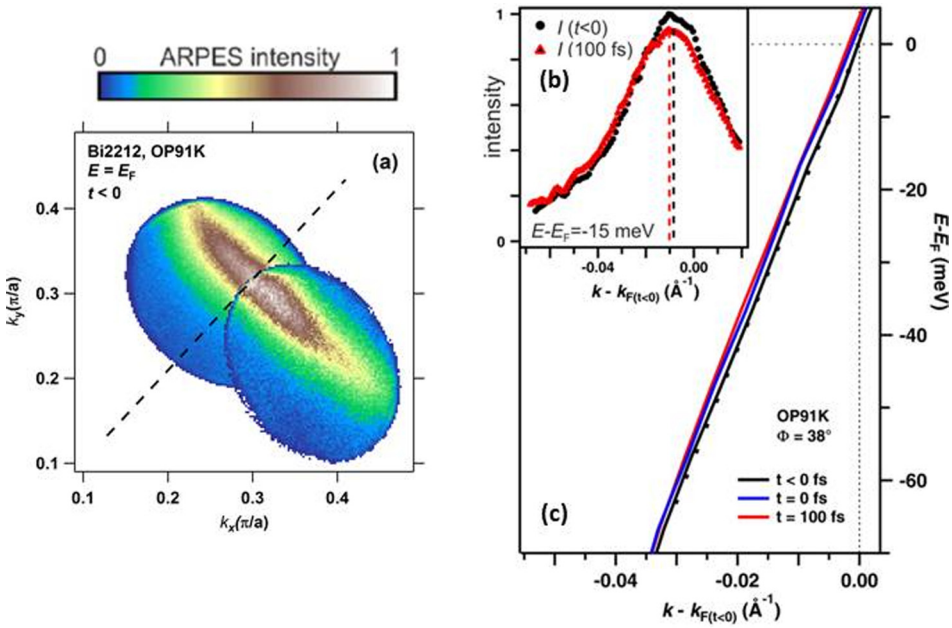


FIG. 2. (a) The spectral intensity measured in the nodal region constructed from two neighboring spectral maps. (b) MDCs showing the measured position of the dispersing band in the nodal direction at a binding energy corresponding to 15 meV at two different times: $t < 0$ before the pump pulse arrives and 100 fsecs after the pump pulse arrives. (c) The extended dispersing band in the nodal direction measured at two time intervals: 0 fs, effectively before the pump, and 100 fs after the pump. Elsewhere [20], we have presented similar data for other time delays.

$200\,\mathrm{mJ/cm^2}$. $\Delta k_F$ is determined by deriving the full band dispersions through energy dependent momentum distribution curve (MDC) peak fittings as a function of angle and time compared with that measured 5 ps before the incident pump pulse. In all cases, the maximum $\Delta k_\mathrm{F}$ occurs approximately 100 fs after excitation with the system subsequently relaxing back to its equilibrium. Particularly in the underdoped case, it is very clear that the instantaneous change in the Fermi wave vector due to the injection of additional photoholes is much larger away from the nodal direction than in the nodal direction, defined by $\varphi = 45^\mathrm{o}$, indicated by the dashed line in Fig. 2(a).

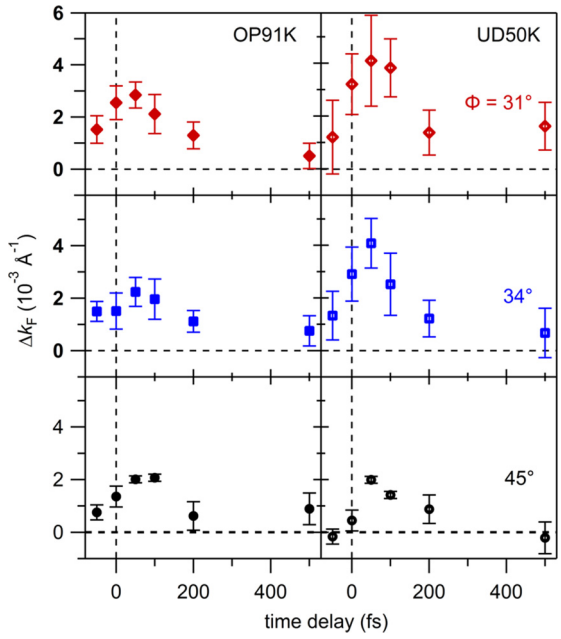


FIG. 3. Measured change in $\Delta k_\mathrm{F}$ as a function of angle and of time delay for two different doping levels as indicated, with OP91 K corresponding to optimally doped with $T_c = 91$ K and UD50 K corresponding to the underdoped material with $T_c = 50$ K. The nodal direction corresponds to an angle of 45°. Note that the error bars were determined by the standard deviation of the linear fit analysis to the $E(k)$ as shown in Fig. 2.

In Fig. 1, we reproduced from Ref. [8] the calculated Fermi surface as a function of doping within the context of the Yang-Rice-Zhang (YRZ) ansatz proposed as a model of the pseudogap state. We note that the YRZ ansatz describes the single-particle Green's function associated with an excitation embedded in a spin-liquid background as in the RVB models. As noted earlier, the ansatz has been shown to provide an excellent description of both the ARPES studies of the hole pockets and of the doping-dependent charge carrier count in YBCO. We make a couple of observations based on the calculation: (a) the change in $k_\mathrm{F}$ with doping is smallest in the nodal direction and (b) the change in $k_\mathrm{F}$ as a function of doping is largest near the ends of the pockets in the underdoped region. The latter observations are also consistent with SISTM studies of the Fermi surface.

In Figs. 4(a) and 4(b), we compare the measured change in the Fermi wave vector at the two different doping levels with the predicted change based on two different pictures of the Fermi surface. The experimental points represent a local average over ±3°. The green dashed lines represent the anticipated change in the Fermi wave vector as a function of angle based on the concept of a full Fermi surface with area proportional to $(1 + x)$, where again $x$ represents the doping level. Here we are simply assuming a circular Fermi surface centered on the $(\pi,\pi)$ point of the Brillouin zone. In this model, the calculated change in the Fermi wave vector $\Delta k_F$, proportional to $\Delta x/k_\mathrm{F}$, is very similar, reflecting the relatively small amount of charge injected. The green dashed line in Figs. 4(a) and 4(b) reflect the isotropic change $\Delta k_\mathrm{F}$ predicted by this model. Thus, within this model, $\Delta k_\mathrm{F}$ in the nodal direction would be larger in the underdoped regime than the optimally doped regime, contrary to the experimental observations for the nodal direction indicated by the green triangles.

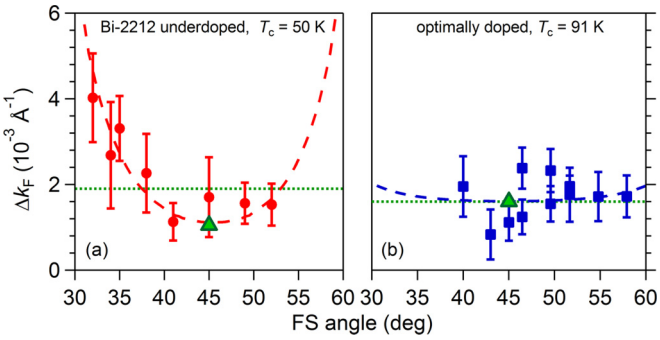


FIG. 4. (a) The closed red dots with associated error bars indicate the measured change in $k_F$ as a function of angle for the underdoped $T_c = 50$ K material. The nodal direction corresponds to an angle of 45°. The experimental measurements are compared with the red dashed line representing the calculated change using the YRZ ansatz and the green dashed line indicating the potential change to be expected in the simple large Fermi surface model. (b) The same as in (a), but now for the optimally doped $T_c = 91$ K material. The blue dashed line is again calculated within the YRZ ansatz.

The second model is based on the use of the YRZ ansatz. Thus in Figs. 4(a) and 4(b), the red and blue dashed lines indicate the change in the calculated Fermi wave vector between two different spectral functions, $A(k, \omega)$, corresponding to the change in doping levels, before and after photoinjection. Here, $A(k, \omega) = -\mathrm{Im}\, G(k, w)$, where

$$G(k, \omega) = \frac{g_t}{\omega - \xi_k - \Delta_R^2[\omega + \xi_0(k)]}, \qquad (1)$$

with $g_t$ a factor that reflects the availability of sites for intersite hole hopping as a function of doping, $\xi_k$ the underlying electronic structure, and $\xi_0$ the nearest-neighbor hopping term. $\Delta_R$ represents the RVB gap function associated with singlet pairing and, in the present case, $\omega$ corresponds to the Fermi energy. Elsewhere we have shown that the doping-dependent term $\Delta_R$ [8,22] derived from the exchange interaction term, $J \sum s_i s_j$ , contained in the $t - J$ model can provide the basis for a mean-field description of the doping-dependent pseudogap temperature, $T^*$ [23]. In the nodal direction, Eq. (1) reduces simply to $g_t/(\omega - \xi_k)$). The distinction between the measured $\Delta k_F$ and the calculated $\Delta k_F$ for the full Fermi surface is observable for the optimally doped system, but could still be argued to be within error bars. However, the deviation from the calculated full Fermi surface $\Delta k_F$ for the underdoped sample is quite dramatic. Good agreement is found for the $\Delta k_F$ associated with the hole pockets, however. We note that the $\Delta k_F$ reported here corresponds to a hole doping at the level of approximately $4.4 \pm 0.2 \times 10^{-3}$ holes per incident photon, in agreement with our earlier study [21].

Here we report that pump-probe studies allow us to observe the deviation of the Fermi surface associated with small hole pockets from that associated with the large Fermi surface that tends to characterize the overdoped regime. This is an interesting observation because "static" photoemission invariably reports that the Fermi arcs associated with the underdoped region always appear to fall on that large Fermi surface [24]. However, we note that in our earlier study which mapped out the shape of the "pockets," it was necessary to normalize the measured spectra to the Fermi distribution and thereby acquire a more accurate measurement of the Fermi surface crossing point [25]. This had the effect of shifting the position in momentum space associated with the Fermi surface, probably reflecting the observation that more weight is given to states just above the chemical potential. In the present study, we pump the system with near-IR photons and monitor the relaxation on ultrafast timescales. Immediately after, i.e., approximately 100 fs, we presumably populate the same states and gain access to the same information.

In summary, we have applied the pump-probe technique to study the nature of the Fermi surface in the underdoped cuprates. These studies clearly confirm the concept of small pockets characteristic of the doped Mott insulator.

This work was funded by the Deutsche Forschungsgemeinschaft through Sfb 616, Sfb 1242 (Project No. 278162697), and SPP 1458, from the Mercator Research Center Ruhr through Grant No. PR-2011-0003 and from the European Union within the Seventh Framework Program under Grant No. 280555 (GO FAST). The work at Brookhaven Laboratory was supported in part by the Center for Emergent Superconductivity (CES), an Energy Frontier Research Center funded by the US Department of Energy, Office of Basic Energy Sciences and in part by the Office of Science, US Department of Energy under Contract No. DE-SC001274.

[1] H. Ding, T. Yokoya, J. C. Campuzano, T. Takahashi, M. Randeria, M. R. Norman, T. Mochiku, K. Kadowaki, and J. Giapintzakis, Nature (London) **382**, 51 (1996).
[2] A. G. Loeser, Z. X. Shen, D. S. Dessau, D. S. Marshall, C. H. Park, P. Fournier, and A. Kapitulnik, Science **273**, 325 (1996).
[3] A. Kanigel, M. R. Norman, M. Randeria, U. Chatterjee, S. Souma, A. Kaminski, H. M. Fretwell, S. Rosenkranz, M. Shi, T. Sato, T. Takahashi, Z. Z. Li, H. Raffy, K. Kadowaki, D. Hinks, L. Ozyuzer, and J. C. Campuzano, Nat. Phys. **2**, 447 (2006)
[4] H. B. Yang, J. D. Rameau, P. D. Johnson, T. Valla, A. Tsvelik, and G. D. Gu, Nature (London) **456**, 77 (2008).
[5] A. Kaminski, T. Kondo, T. Takeuchi, and G. Gu, Philos. Mag. **95**, 453 (2015).
[6] H.-B. Yang, J. D. Rameau, Z.-H. Pan, G. D. Gu, P. D. Johnson, H. Claus, D. G. Hinks, and T. E. Kidd, Phys. Rev. Lett. **107**, 047003 (2011).
[7] X. G. Wen and P. A. Lee, Phys. Rev. Lett. **80**, 2193 (1998).
[8] K. Y. Yang, T. M. Rice, and F. C. Zhang, Phys. Rev. B **73**, 174501 (2006).
[9] Y. Qi and S. Sachdev, Phys. Rev. B **81**, 115129 (2010).
[10] I. R. Dzyaloshinskii, Phys. Rev. B **68**, 085113 (2003).
[11] J. Zaanen, G. A. Sauatzky, and J. W. Allen, Phys. Rev. Lett. **55**, 418 (1985).

[12] P. A. Lee, Rev. Mod. Phys. **78**, 17 (2006).
[13] K. Fujita, Chung Koo Kim, Inhee Lee, Jinho Lee, M. H. Hamidian, I. A. Firmo, S. Mukhopadhyay, H. Eisaki, S. Uchida, M. J. Lawler, E.-A. Kim, and J. C. Davis, Science **344**, 612 (2014).
[14] S. Badoux, W. Tabis, F. Laliberté, G. Grissonnanche, B. Vignolle, D. Vignolles, J. Béard, D. A. Bonn, W. N. Hardy, R. Liang, N. Doiron-Leyraud, L. Taillefer, and C. Proust, Nature (London) **531**, 210 (2016).
[15] S. Benhabib, A. Sacuto, M. Civelli, I. Paul, M. Cazayous, Y. Gallais, M.-A. Méasson, R. D. Zhong, J. Schneeloch, G. D. Gu, D. Colson, and A. Forget, Phys. Rev. Lett. **114**, 147001 (2015).
[16] J. L. Tallon, F. Barber, J. G. Storey, and J. W. Loram, Phys. Rev. B **87**, 140508 (2013).
[17] T. L. Miller, W. Zhang, H. Eisaki, and A. Lanzara, Phys. Rev. Lett. **118**, 097001 (2017).
[18] P. S. Kirchmann, L. Rettig, D. Nandi, U. Lipowski, M. Wolf, and U. Bovensiepen, Appl. Phys. A **91**, 211 (2008).
[19] P. W. Anderson, Science **235**, 1196 (1987); P. W. Anderson, P. A. Lee, M. Randeria, T. M. Rice, N. Trivedi, and F. C. Zhang, J. Phys.: Condens. Matter **16**, 755 (2004).
[20] M. R. Norman and J. C. Davis, Proc. Natl. Acad. Sci. USA **115**, 5389 (2018).
[21] J. D. Rameau, S. Freutel, L. Rettig, I. Avigo, M. Ligges, Y. Yoshida, H. Eisaki, J. Schneeloch, R. D. Zhong, Z. J. Xu, G. D. Gu, P. D. Johnson, and U. Bovensiepen, Phys. Rev. B **89**, 115115 (2014).
[22] K.-Y. Yang, H.-B. Yang, P. D. Johnson, T. M. Rice, and F.-C. Zhang, Europhys. Lett. **86**, 37002 (2009).
[23] N. Zaki, H. B. Yang, J. D. Rameau, P. D. Johnson, H. Claus, and D. G. Hinks, Phys. Rev. B **96**, 195163 (2017).
[24] H. Ding, M. R. Norman, T. Yokoya, T. Takeuchi, M. Randeria, J. C. Campuzano, T. Takahashi, T. Mochiku, and K. Kadowaki, Phys. Rev. Lett. **78**, 2628 (1997).
[25] Supplemental Material for Ref. [6].